Cellular & Molecular

Counting Ion and Water Molecules in A Streaming File through the Open-Filter Structure of A K Channel

*Masayuki Iwamoto & Shigetoshi Oiki**
Department of Molecular Physiology and Biophysics, University of Fukui Faculty of Medical Sciences, 23-3 Matsuokashimoaizuki, Eiheiji-cho, Yoshida-gun, Fukui 910-1193, Japan

Abstract
Mechanisms underlying selective permeation of ions through channel molecules are a fundamental issue to understand how neurons operate their function. The knock-on mechanism, in which multiple ions in the selectivity filter are hit by an incoming ion, is one of the leading concepts. This mechanism has been supported by crystallographic studies that demonstrated ion distributions in the structure of the KcsA potassium channel. These still pictures under equilibrium conditions, however, may not be a snapshot of on-going permeation processes. To understand dynamics of permeation, here we counted the ratios of ion and water flow (the water-ion coupling ratio: $CR_{w\text{-}i}$) through the KcsA channel by measuring the streaming potential (V_{stream}) electrophysiologically. Water flow driven by the osmotic pressure flushes out ions in the narrow selectivity filter and generates potential differences across the membrane (V_{stream}). The V_{stream} value was converted to the $CR_{w\text{-}i}$ value, which tells us how individual ion and water molecules are queued in the narrow and short filter during permeation. At high K^+ concentrations, the $CR_{w\text{-}i}$ value was 1.0, indicating that turnovers between the alternative ion and water arrays in a single-file undergoes. At low K^+, the $CR_{w\text{-}i}$ value was increased over 2.2, suggesting that the filter contained mostly one ion at a time. These average behaviors of permeation were kinetically analyzed for more detailed permeating processes. Here we envisioned the permeation as queues of ion and water and sequential transitions between different patterns of arrays. At physiological conditions, we predicted that the "knock-on" mechanism may not be predominant.

KEYWORDS. Streaming potential, Water-ion coupling ratio, Single-file permeation, Cycle flux, Osmotic jump method.

Introduction

Ion channels mediate ion flux with the high throughput rates, while retaining strict selectivity (Hille, 2001). The mechanism underlying selective permeation is a fundamental issue of neurosciences and has been studied extensively for several decades. Among them, Hodgkin and Keynes (Hodgkin and Keynes, 1955) proposed an insightful mechanism referred to knock-on, which has relived in the present scientific scene.

The crystal structure of potassium channels revealed a narrow and short stretch of the selectivity filter (Fig. 1A), where ions and water molecules cannot pass each other (single-file permeation). Multiple ions and water molecules occupy defined sites in the filter under equilibrium conditions (Doyle et al., 1998; Morais-Cabral et al., 2001; Zhou et al., 2001). These distribution patterns provoked the clear image that during permeation the ion and water generate a queue and the ratio of the ion and water molecules undergoing permeation are thus countable.

MacKinnon's group (Morais-Cabral et al., 2001; Zhou and MacKinnon, 2004) deciphered the permeation process as transitions between two alternative arrays having ions and water molecules aligned one after the other, i.e., *i*-*w*-*i*-*w* and *w*-*i*-*w*-*i* (where *i* and *w* represents the ion the water molecules). These ion-distribution states were integrated into a discrete-state permeation model to express the permeation kinetics and the 8-state model became a canonical model for the K channels (Fig. 1B). Decoding the dynamic pattern of permeating queues from the still pictures was a most sophisticated achievement of the permeation study. There is, however, a pitfall in this scenario. Permeation is intrinsically a dynamic process, while a crystal structure, being frozen, necessarily gives an ensemble average of the equilibrium structure.

Here we present an approach to study dynamic processes of ion permeation through the open-filter structure during steady-state permeation. In the ion channel, the high throughput rate of ion conduction accompanies water flux in a comparable order (Hille, 2001). This high water flux is mandatory in a narrow no-pass pore, and we exploited this coupled water flux to understand underlying processes of permeation.

To gain realistic pictures of permeation, one watches the exit of the selectivity filter with an imaginary microscope, taking a view point of Maxwell's demon sits at the exit (Fig. 1D). The demon finds that the output flow from the selectivity filter is constituted of a queue of ion and water molecules, and is able to count individual particles. This queue is generated in the selectivity filter, where ion and water move by jumping state-to-state among the 8 possible ion and water configurations (Fig. 1B). There are many cyclic paths on the diagram and each cycle carries a defined number of ion and water molecules, such as 1:1, 2:1, etc. (Fig. 1C). Thus, transitions among cycles reflect the counted ratio of ion and water. Even without having such microscope, the water-ion coupling ratio ($CR_{w\text{-}i}$ = J_{water}/J_{ion}; J_{water} and J_{ion} represent the flux of water and ion molecules per second) (Katchalsky and Curran, 1965; Schulz, 1980; Miller, 1982; Alcayaga et al., 1989; Dani, 1989; Ando et al., 2005; Oiki et al., 2010) can be measured electrophysiologically using the streaming potential.

Experiments were performed for the KcsA potassium channel since various crystal structures exhibiting different ion distributions are available. We observed changes in the $CR_{w\text{-}i}$ value at different K^+ concentrations. These $CR_{w\text{-}i}$ value were related to underlying permeation processes using a theoretical method (Oiki et al., 2011). Here we envisioned how ion and water molecules are queued during permeation and predicted how they are modified in physiologically relevant conditions.

Materials and Methods

Preparation of KcsA-reconstituted giant unilamellar vesicles (GUVs)

The expression and purification of the KcsA channel were described previously (Iwamoto et al., 2006). The KcsA-reconstituted GUVs were

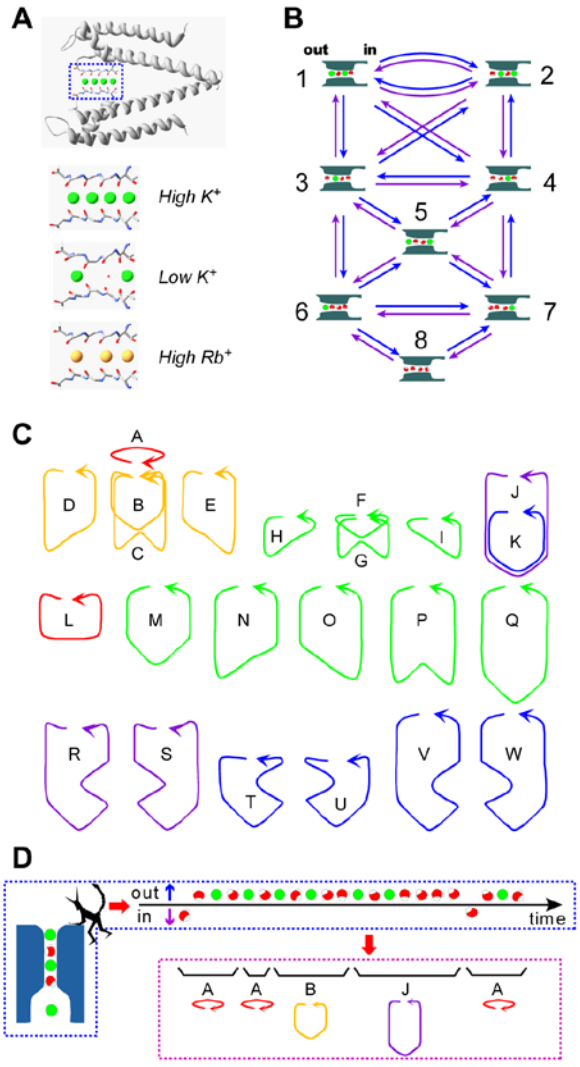

Fig. 1. Permeation processes through the KcsA channel.
A. The equilibrium ion distribution in the crystal structure of KcsA channel. The selectivity filter (boxed region of the upper panel) was enlarged in the lower panel at different ionic conditions (PDB code: 1k4c, 1k4d and 1r3i). There are four ion-binding sites in the selectivity filter, and the binding sites are called S1 to S4 from outside (left) to inside. The filter structure is collapsed at low K^+ concentration. Even at high concentration of Rb^+, S2 site is left unoccupied. **B.** The discrete-state permeation model for the KcsA channel. The model involves eight K^+ (green)-water (red) occupied states (cartoons with the state number; The left side is the extracellular space.) in the selectivity filter, and transitions among them (arrows). The blue arrows indicate transitions for efflux and the violet ones for influx. **C.** The cyclic paths on the permeation diagram. For example, cycle *A* represents transitions between state 1 and 2, and cycle *F* represents transition around state 3, 4 and 5. There are 23 cyclic paths for ion flux (alphabetical). They all involve two one-way cyclic paths with opposite directionality. The arrows indicate cycle direction for efflux (defined as + cycles). The cyclic paths are color coded representing the water-ion coupling ratio. The red cycles represent 1:1 (water : ion) flux ratio, yellow for 3:2, green for 2 : 1, violet for 5 : 2, blue for 4 : 1. **D.** A queue of ion and water flux and cycles on the diagram. From the observed queue of ion and water, the demon assigned the queue to a series of cycles. Thus, ion and water flux can be regarded as random transitions among cycles.

prepared according to the usual protocols (Delcour et al., 1989; Cortes et al., 2001) with some modification. Purified KcsA channels (~1 mg/mL) were reconstituted into azolectin (type IV-S; Sigma, St. Louis, MO) liposomes with a protein/lipid weight ratio of 1 : 50. The proteoliposomes (~5 mg) were collected by centrifugation (18,800 × g, 2 hr) and resuspended in 100 μL of 10 mM Hepes (pH 7.5) containing 5% ethylene glycol. 5 μL of the suspension was dried for 6 hours under vacuum on a clean cover glass surface. The dehydrated lipid film was rehydrated by 5 μL of the rehydration buffer (100 mM KCl, 1 mM $MgCl_2$, 10 mM Hepes pH 7.5). GUVs suitable for the electrophysiological measurement were obtained after overnight rehydration at room temperature.

Apparatus for V_{stream} measurement by osmotic jump method

The electrophysiological setup and the ultrafast solution exchange system for the osmotic jump method were the same as those reported previously (Ando et al., 2005; Kuno et al., 2009), except for the configuration of the reference electrode. The reference electrode was set adjacent to the patch pipette electrode during the osmotic jump experiment. In this configuration, we were able to avoid the establishment of a liquid junction potential between the two electrodes because they were always in the same solution (outflow).

Determination of the V_{stream} value

The voltage command and the positioning of the double (or triple) barrel tube, from which the desired bathing solutions flowed out, were under the control of the program (Fig. 3A). The series of ramp command was applied (Fig. 3E), and thirty *I-V* curves were obtained. To evaluate the V_{stream} values, linear regression of time-dependent changes of V_{rev} during the hyper-osmotic pulse was performed, and the regression line was extrapolated to the time of an osmotic jump. Then, the values at the moment of the establishment of ΔOsm across the membrane were defined as the V_{stream} (Fig. 3G) (Ando et al., 2005). The osmolalities of the solutions were measured with an osmometer (Osmostat OM-6040; Arkray, Kyoto, Japan) and adjusted to the desired values by adding sorbitol. K^+ or Rb^+ activity for the pipette solution and corresponding bathing solutions (outflows from barreled tube) were adjusted to the same values by using a potassium-selective electrode (Model 971901; Thermo Scientific, Waltham, MA).

The diagram method for the cycle flux

The 8-state permeation diagram (Fig. 1B and 2A) was similar to that proposed by Molais-Cabral et al. (Morais-Cabral et al., 2001), in which either an ion or a water molecule occupies one of the four binding sites, and two ions are not allowed to occupy adjacent positions because of electrostatic repulsion. The 13 rate constants were set assuming that the potential profile of the permeation for K^+ is symmetrical. Hereafter we call this model as the canonical 8-state model.

The steady-state probability of the states was calculated using the conventional method (Colquhoun and Hawkes, 1995). On the other hand, the net ion flux for the complicated 8-state model needs cycle flux (the rate of completing a cycle) calculation. Given the cycle flux, $CR_{w\text{-}i}$ is readily calculated. The method for calculating the cycle flux is briefly described (Oiki et al.,

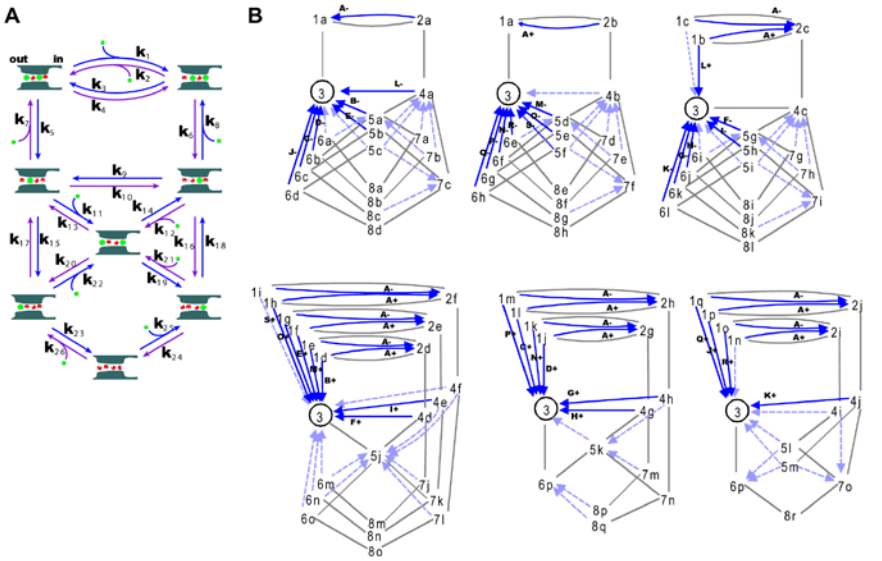

Fig. 2. A discrete state permeation diagram and the expanded diagram for the KcsA channel. **A.** The permeation diagram used in this study with the name of rate constants. This model involves cycles having different $n_{w\text{-}i}$ values. **B.** The expanded diagram. The expanded diagram was constructed by defining state 3 as the starting state and all the state, except for state 3, were subdivided into substates, such as substate 8c, etc. These diagrams include all 48 cyclic paths with one-way directionality (the expanded diagram). The arrows indicate the completing transitions for the one-way cycles, in which the solid arrows represent those of generating the net cycle flux, and the cycle names are indicated with the + or - sign. The broken arrows indicate cycles of no net cycle flux. From the diagram, one-way cycle fluxes for all the cyclic paths are readily calculated from matrix algebra.

2011).

For a permeation diagram, the graphical procedure leads to the drawing of the expanded diagram (Fig. 2B), in which all of the cyclic paths in the original diagram having reversible plus (efflux) and minus (influx) cyclic fluxes are decomposed into one-way cyclic paths having distinct routes on the expanded diagram (Hill, 2004). The initial procedure is to draw the tree diagrams (gray lines in Fig. 2B), where all of the states are visited once without forming cycles. The states on the original diagram appear on each tree diagram, and they should be distinguished from each other by assigning the sub-state name (e.g., substates 8a-8r). From an end state of the branched paths, a one-way arrow (blue) is drawn to a state upstream of the tree branching. This generates a one-way cyclic path, and continuing this procedure generates the expanded diagram (Fig. 2B).

From the expanded diagram the transition matrix is formulated, such that the transition rate between the sub-states is assigned to be the same as that of the states on the original diagram. The total number of the sub-states was 100, and a 100 × 100 matrix was generated. The steady-state probabilities of the sub-states were readily calculated numerically from the matrix inversion.

On the expanded diagram, each arrow represents the completing transition for a one-way cyclic path, and the one-way cycle flux is calculated as the product of the probability of the sub-state at the tail of the arrow and the rate constant assigned for the arrow. For the case in which multiple arrows are involved in a cycle, these products were summed up. The cycle flux is defined by the one-way cycle fluxes of both directions ($J_{\kappa} = J_{\kappa+} - J_{\kappa-}$). Finally, for each cycle path, the stoichiometric numbers of the ion and water transfer were assigned (n_i, n_w and $n_{w\text{-}i}$)(Ando et al., 2005), and the net ionic current and $CR_{w\text{-}i}$ were calculated (Oiki et al., 2011).

The optimization of the rate constants

Three different kinds of experimental data ($CR_{w\text{-}i}$, conductance and ion occupancy) were used for optimizing the rate constants of the permeation model.

Estimation of the water-ion coupling ratio contributed from the wide pore region

Osmotically driven water flux in the wide pore region outside of the single-file selectivity filter carries ions and this may contribute to the measured $CR_{w\text{-}i}$. Levitt proposed a theoretical method to estimate the water-ion coupling in the wide pore region based on the continuum theory (Levitt, 1990).

$$vol = 6\eta a L L_p \frac{1-1.33\alpha^2}{hR^2} \qquad \text{Eq. 1}$$

where *vol* is the volume associated with the passage of one ion through the wide pore, η is the viscosity, a the ion radius, L the length of the wide pore, L_p the hydraulic water conductivity of the rate-limiting process in the pore, R the radius of the wide pore, α the a/R, and

$$h = 1 - 2.1054(a/R) + 2.0805(a/R)^3 \qquad \text{Eq. 2}$$

By dividing the *vol* by the volume of a water molecule, the water-ion coupling in the wide pore region is calculated.

For the intracellular entryway towards the central cavity for the open structure of KcsA, the crystal structure gives the geometry of about 5-6 Å in the radius, and 25 Å in the length (Cuello et al., 2010). In the Levitt equation, the L_p for the rate-limiting conduction step is used to represent the water flux in the entire pore, and the L_p value of the selectivity filter should be used. Dani and Levitt (Dani and Levitt, 1981) further defined L_p as,

$$L_p = f_0 L_0 + f_1 L_1 + f_2 L_2 + ... \qquad \text{Eq.3}$$

where f_0, f_1, f_2 etc. are the fraction of channels that contain zero, one, two, etc. ions and L_0, L_1, L_2 etc. are the hydraulic water conductivity for channels containing zero, one, two, etc. ions. In the experimental condition for measuring the streaming potential, however, L_1 and L_2 are ignored since water flux for the ion occupied pores are stopped in the zero current condition, and only the L_0 value is valid for calculating the L_p value (Dani and Levitt, 1981). For f_0, the probability of the channel being in the empty filter (state 8) is calculated from the permeation diagram with the optimized rate constants, Given the L_0 value, the water-ion coupling ratio in the wide pore can be estimated once the f_0 value is obtained.

Results

KcsA channel currents and the streaming potential revealed by the osmotic pulse method

In the narrow pore where single-file permeation is undergoing, ion flow drives water flow and vice versa. Even in the absence of the electrochemical potential differences for a permeating ion, the net water flow driven by the osmotic difference across the membrane generates the net ion flow. The generated membrane

potential is referred to the streaming potential (V_{stream}) (Miller, 1982; Alcayaga et al., 1989; Dani, 1989; Ismailov et al., 1997; Ando et al., 2005) and provides prerequisite information of underlying permeation processes encompassing how ion and water molecules are queued.

To measure the streaming potential, the KcsA channel was reconstituted into giant unilamellar vesicles (GUV) and patch-clamping was performed (Chakrapani et al., 2007)(see Methods). A GUV membrane, on which the channels are oriented with the cytoplasmic domain inside (Chakrapani et al., 2007), was excised and the inside-out membrane was exposed to acidic pH to elicit single and macroscopic channel currents (Fig. 3B-D). A train of thirty ramp voltages was applied (Fig. 3E) (Ando et al., 2005), and during the middle ten ramps in a train, the patch membrane was exposed to a hyper-osmotic solution (1 to 3 Osm/kg H_2O sorbitol; ΔOsm) for one second using a rapid perfusion system (Fig. 3A) (Ando et al., 2005). Fig. 3E shows a representative current trace in a train. From the current traces during the ramp voltage, the *I-V* curves were drawn (Fig. 3F) and the reversal potential (V_{rev}) was measured. A typical time course of the changes in the V_{rev} values before, during and after an osmotic pulse is depicted in Fig. 3G. After the stable V_{rev} recordings under the steady iso-osmotic condition, V_{rev} jumped towards a positive potential upon the hyper-osmotic pulse. A gradual but significant positive shift of V_{rev} during the hyper-osmotic pulse and reversal of V_{rev} upon returning to the iso-osmotic solution were observed. The gradual shifts are consistent with our previous report for

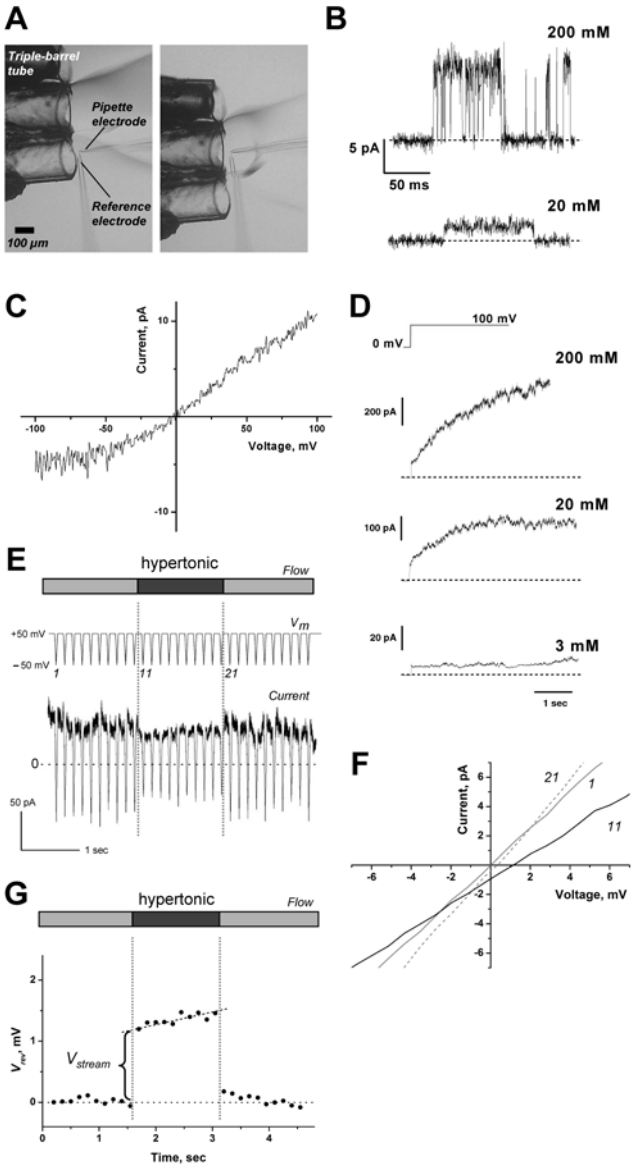

Fig. 3. Measurements of the KcsA currents and the streaming potential. **A.** The osmotic pulse method. Configuration of perfusion tubes and electrodes are shown. The outflow from each tube is different in osmolality. Rapid positional shifts of the tube lead to generate osmotic jumps within a several ms. The patch was stable even as it endured a 3 Osmolar gradient (ΔOsm) across the membrane. **B.** Single-channel current of the KcsA channel at different K^+ concentrations at pH 4.0. The current was measured at +100 mV. **C.** Single-channel current-voltage curve. A ramp voltage from -100 to +100 mV was applied during open and closed states and the difference current was drawn. **D.** Macroscopic current upon voltage steps from 0 mV to +100 mV. The KcsA channel exhibits slow activation at positive potentials, and the time course of the activation differs significantly at different K^+ concentrations. **E.** The protocol and evaluation of the V_{rev}. A train of the ramp voltage (+50 to −50 mV) was applied before, during and after the osmotic pulse. A representative current trace elicited by a train of ramp commands synchronized with an osmotic pulse (in this case, 2.0 Osm / kg H_2O) is shown in symmetric 200 mM K^+ at pH 4.0. A slight reduction in current amplitudes was observed during exposure to the hyper-osmotic solution. This reduction seems to occur at the access resistance, that was augmented by the hyperosmotic solution having the higher resistivity (Kuno et al., 2009). **F.** The shifts of the *I-V* curves during the time course of the osmotic pulse. The *I-V* curves were drawn from the ramp current. The numbers on the *I-V* curves represent the number of the ramp command. V_{rev} was obtained by linear regression of *I-V* curves. **G.** A typical time course of V_{rev} during the command train. Osmotically driven water flux across the membrane towards the outside of the pipette leads to the condensation of K^+ at the inner surface of the patch membrane, which generates the gradual positive shifts of V_{rev} during the hyper-osmotic period.

the HERG channels (Ando et al., 2005), and originated from changes in the local K^+ concentration at the surface of the patch membrane. The V_{stream} value was determined from the jump of V_{rev} values at the beginning of the osmotic pulse (Fig. 3G).

Evaluation of the water-ion coupling ratio and the permeation model

Fig. 4A shows the ΔOsm-dependency of V_{stream} for the KcsA channel in 200 mM K^+. V_{stream} and ΔOsm exhibited a linear relationship. The slope value of 0.45 ± 0.03 mV/ΔOsm was obtained from linear regression of the plots. This value is smaller than those ever measured. Such precise measurements of ours rely on the setting of the appropriate reference points, such as the reference electrode and evaluation of the immediate V value relative to the pre-jump (iso-osmotic) value (Materials and Methods), while earlier methods needed corrections for several independent experimental parameters to reach the final results.

The following equation relates the slope value to the ratio of the water flux (J_w) and the ion flux (J_i) (the water–ion coupling ratio, $CR_{w\text{-}i}$) (Levitt et al., 1978; Rosenberg and Finkelstein, 1978):

$$CR_{w-i} = \frac{J_w}{J_i} = -\frac{V_{stream}}{\Delta\pi}\frac{zF}{v_w} \quad \text{Eq. 4}$$

where $\Delta\pi$ is the osmotic pressure; v_w, the molar volume of water; z, the valence of ion; and F, the Faraday constant. The $CR_{w\text{-}i}$ was determined to be 1.0 at 200 mM K^+.

$CR_{w\text{-}i}$ for Rb^+ and K^+ at different concentrations

Next, we evaluated the V_{stream} in Rb^+ solutions since Rb^+ is known to permeate K channels with unusual conduction features (Eisenman et al., 1986; Hille, 2001; LeMasurier et al., 2001). Fig. 4B shows ΔOsm-dependency of V_{stream} in 200 mM Rb^+. The slope value for Rb^+ permeation (0.94 ± 0.08 mV/ΔOsm) was significantly higher than that for K^+. The $CR_{w\text{-}i}$ value was 2.0, indicating that two water molecules were carried with one Rb^+ ion. The asymmetric distribution of Rb^+ in the crystal structure (Fig. 1A) (Zhou et al., 2001; Lockless et al., 2007) and an interpretation posed by Morais-Cabral et al. that state 2 (Fig. 1B) might be destabilized in the energy profile of the permeation (Morais-Cabral et al., 2001) are consistent with our data.

Figs. 4C and D show ΔOsm-dependency of V_{stream} in the low K^+ concentrations. From the slope values the $CR_{w\text{-}i}$ was evaluated to be 1.8 and 2.2 in 20 and 3 mM K^+, respectively. The results clearly indicate that the number of water molecules in a queue increased substantially at low K^+. In this way, we have experimentally counted the ion and water molecules in a streaming file through the open-filter structure of the KcsA channel.

The cycle flux and the $CR_{w\text{-}i}$ value

From the measured $CR_{w\text{-}i}$ values, one may attain more intuitive insights on the underlying permeation process. The permeation has been represented as random transitions among the ion-water occupied states on the discrete-state permeation model (Lauger, 1980; Miller, 1999) (Fig. 1B)(Morais-Cabral et al., 2001). On the permeation diagram, there are many cyclic paths (Fig. 1C). Starting from an arbitrary state, back and forth random transitions spontaneously return to the starting state and complete a cycle. For example, starting from state 3, transitions undergoes through a route such as 3 → 4 → 5 → 3 and forms cycle F. By completing this cycle the number of water molecules (n_w) and ions (n_i) are carried (the ratio is n_w/n_i). Experimentally obtained $CR_{w\text{-}i}$ values are, thus, best related to contribution of cyclic paths on the diagrm, in which each path exhibits a defined number of coupled ion and water transfers.

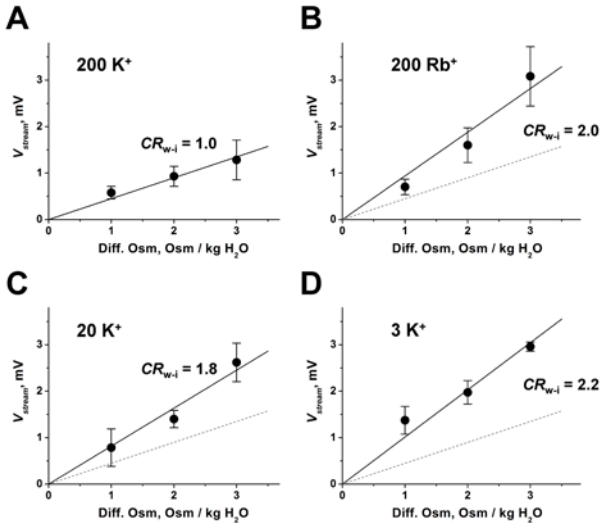

Fig. 4. The streaming potential of the KcsA channel. ΔOsm-dependency of V_{stream} under various ionic conditions. From the slope, the $CR_{w\text{-}i}$ value was calculated. The slope values were 0.45 ± 0.03 mV/ΔOsm for 200 mM K^+ (A) and 0.94 ± 0.09 mV/ΔOsm for 200 mM Rb^+ (B), 0.82 ± 0.05 and 1.01 ± 0.07 mV/ΔOsm in 20 mM (C) and 3 mM K^+ (D). The data represent the mean slope value ± the error of the slope.

One can measure the cycle completion rate (cycle flux) by counting how many times the random walk returns to an arbitrary state through a defined cyclic route in a given time (Hill, 1988; Oiki et al., 2011). The completion of each cycle can be regarded as an independent event, and the sum of the cycle fluxes generates the net flux (Fig. 2).

$$J_{net} = J_A + J_B + J_C + \ldots \qquad \text{Eq. 5}$$

where J_κ is the cycle flux for cycle κ.

Each cyclic route (Fig. 1C) has its distinct stoichiometric number for ion (n_i) and water (n_w) fluxes (Ando et al., 2005; Oiki et al., 2011). Thus, the stoichiometric ratio, n_w/n_i (the water-ion ratio: $n_{w\text{-}i}$), for each cycle can be defined, and these values of all the cycles in the diagram determine the $CR_{w\text{-}i}$ value.

$$CR_{w-i} = n^A_{w-i}\frac{J_A}{J_{net}} + n^B_{w-i}\frac{J_B}{J_{net}} + n^C_{w-i}\frac{J_C}{J_{net}} + \ldots \qquad \text{Eq. 6}$$

where $n_{w\text{-}i}{}^A$, $n_{w\text{-}i}{}^B$ and $n_{w\text{-}i}{}^C$ are the water-ion stoichiometry for the cycles *A*, *B* and *C* (Oiki et al., 2011). For example, if permeation undergoes predominantly by transitions between state 1 and 2, it generates a cyclic path of cycle *A* (Fig. 1B,C). Upon completion of cycle *A*, one ion and one water molecule are transferred. Cycle *F*, for another example, transfers one ion and two water molecules. If the $CR_{w\text{-}i}$ value is 1.5, cycle *A* and cycle *F* and other cycles are mixed.

Based on the above theoretical consideration, the observed $CR_{w\text{-}i}$ value can be interpreted as to which cycles were predominantly used for a given condition. In the high K^+ (200 mM) condition, the $CR_{w\text{-}i}$ value of 1.0 indicates that cycle *A* having the $n_{w\text{-}i}$ value of one (Fig. 1C) operates predominantly. The gradual increase in the $CR_{w\text{-}i}$ value at lower K^+ concentrations indicates that the predominant cyclic paths are shifted from cycle *A* to other cycles having higher $n_{w\text{-}i}$ values. At 20 mM, cycles having the $n_{w\text{-}i}$ value of 2, such as cycle *F* to *I*, should contribute to the flux. At 3 mM, the $CR_{w\text{-}i}$ value of 2.2 can be attained only if cycles *J*, *K* and others with high $n_{w\text{-}i}$ values (cycles *R*-*W*) are used. These semi-quantitative clues will be extended by relating the $CR_{w\text{-}i}$ values to the underlying process of permeation quantitatively through the cycle flux calculation (Oiki et al., 2011).

Model optimization based on the $CR_{w\text{-}i}$ values

T. L. Hill developed a diagrammatic method to calculate the cycle flux from the rate constants of the relevant permeation diagram (Hill, 1988; Hill, 2004). For a relatively complicated diagram of KcsA channel, we have established a method to relate the rate constants and the cycle flux (Fig. 1B) (Oiki et al., 2011). Using the cycle flux, $CR_{w\text{-}i}$ was eventually expressed with the set of rate constants. The net ionic current was also calculated from the cycle flux, which has otherwise been estimated by the Monte Carlo simulation (Morais-Cabral et al., 2001). Conversely, the rate constants were estimated from the experimental observables through fitting.

To optimize the rate constants, not only the $CR_{w\text{-}i}$ values but also the conductance data (LeMasurier et al., 2001) were used. Also, the K^+ distribution in the filter at only the high concentration (Zhou et al., 2001) were included for optimizing the rate constants. Three different kinds of experimental data thus provided effective constraints for the optimization (Materials and Methods). The $CR_{w\text{-}i}$ values were well reproduced as a function of the K^+ concentration using the optimized rate constants (Fig. 5A). The calculated current amplitudes and the ion-occupancy probability fit the experimental data well (Fig. 5B,C).

Before inquiring the meaning of the $CR_{w\text{-}i}$ values, possible contribution of the wide pore region on the measured $CR_{w\text{-}i}$ values must be taken into consideration. Osmotically-driven water flow carries ions even outside of the single-file pore (Materials and Methods), and here we can estimate the contribution of the wide pore to the measured $CR_{w\text{-}i}$ values. Based on the Levitt equation (Eq. 3), the L_p value for the empty selectivity filter (L_0) is necessary, while f_0 is calculated from the fitted rate constants as the probability of the empty pore (state 8) at given conditions. For the KcsA channel the L_p value is available (Saparov and Pohl, 2004), and their L_p value represents that of the selectivity filter. However, the extremely high L_p value, overwhelming the rest of the pore, does not satisfy the requirement of Eq. 1, in which the rate-limiting L_p value should be used. To approximate a realistic value of the contribution of the entryway, we adopted the L_p values for the gramicidin channels exhibiting single-file permeation (Levitt, 1984). Given the P_f value of 6.0×10^{-14} cm^3/s for L_0 ($L_p = (v_w/RT)\,P_f$; (Dani and Levitt, 1981)), and the probability of the empty channels (2.5×10^{-5} for 200 mM K^+ and 0.044 for 3 mM K^+), the coupling ratio in the wide pore was estimated to be 6.1×10^{-6} at 200 mM K^+ and 0.01 at 3 mM K^+. As far as the rate-limiting L_p value for the KcsA channel is in the similar order of magnitude as that

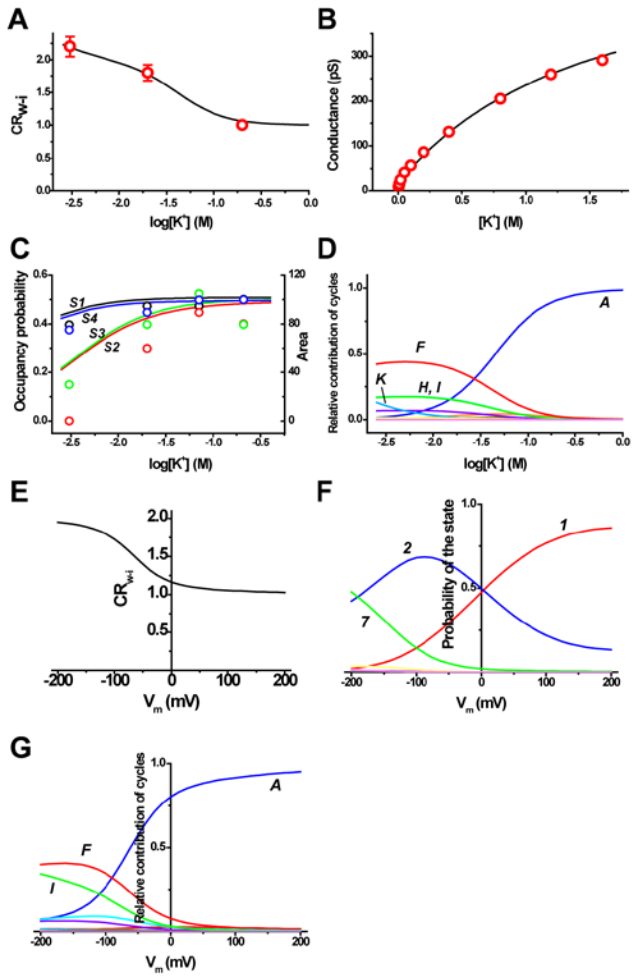

Fig. 5. Experimental data and underlying permeation processes. **A-B.** The experimental data of $CR_{w\text{-}i}$ (A) and the conductance (B) as a function of K^+ concentration. The rate constants of the 8-state permeation model were optimized to fit these experimental data. The lines indicate fitted lines calculated from the cycle flux. **C.** The K^+ occupancy on the four binding sites in the selectivity filter as a function of K^+ concentration. The ion distribution data of the crystal structure represented as the area of the electron density are superimposed through an appropriate scaling. The black color indicates the S1 site, red for S2, green for S3 and blue for S4. **D.** Current contributions from each cycle. The optimized rate constants were: $k_1 = 5.0 \times 10^7$, $k_3 = 1.5 \times 10^8$, $k_5 = 2.5 \times 10^5$, $k_7 = 8.0 \times 10^8$, $k_9 = 3.5 \times 10^8$, $k_{11} = 3.6 \times 10^{10}$, $k_{13} = 1.0 \times 10^9$, $k_{15} = 1.8 \times 10^{10}$, $k_{17} = 1.8 \times 10^9$, $k_{19} = 4.0 \times 10^8$, $k_{21} = 1.44 \times 10^7$, $k_{25} = 2.0 \times 10^6$, $k_{27} = 2.0 \times 10^9$ (/s). **E-G.** Predicted features of permeation in an asymmetric condition of 4 mM K_{out} and 150 mM K_{in} at different membrane potentials. Predicted curves for $CR_{w\text{-}i}$ (E). The probability of states (F). The relative contributions of cycles at different membrane potential (G).

of the gramicidin channel, the $CR_{w\text{-}i}$ value contributed from the wide pore region is negligible.

Now the permeation-related parameters are estimated from the fitted rate constants. At the K^+ concentration of 3 mM, the occupancy probability of K^+ ions in the selectivity filter in the steady-state was 0.44, 0.24, 0.24, and 0.44 at S1, S2, S3 and S4 sites (Fig. 5C; Fig. 1A). On the other hand, the relative ion occupancy deduced from the area of the electron density in the crystal data differs significantly from those of the predicted values as the K^+ concentration decreased. It is now established that the filter structure is collapsed at low K^+ (Zhou et al., 2001), and ion distributions in the non-conductive conformation are irrelevant for understanding the permeation mechanism. Our values reflect the ion occupancy under ongoing permeation through the open-filter structure.

Visualization of permeation processes

From the cycle flux, the relative contributions of the current carried by the cycles were calculated as a function of the K^+ concentration (Fig. 5D). In Fig. 6A, the net flux is visualized as random transitions among cyclic paths, and the relative contribution of each cycle flux is represented as the height of the cyclic paths raised from the footprint. At 200 mM K^+, cycle *A* (dark blue diamond) contributed predominantly to the net flux. In the concentration mid-range, cycle *F* (red triangle) passing through state 5 (the double occupancy state at both ends; Fig. 1B) overwhelmed cycle *A*, and cycle *H* (light blue triangle) and *I* (green triangle) contribute significantly. Below 3 mM, not only cycle *F* but other cycles (cycle *K*; blue escutcheon) significantly contribute to the net current.

Using the optimized set of the rate constants, we predicted permeation features at physiologically relevant asymmetric ion concentrations, such as a 4 mM extracellular K^+ concentration and 150 mM intracellular concentration (Fig. 5E-G, Fig. 6B). We found two things. At 0 mV, the contribution of the cycles in the asymmetric condition (Fig. 6B) is similar to that at the symmetrical 200 mM K (Fig. 6A). At first, this result was counter intuitive since the high K^+ solution on one side governs the distribution exclusively. As the membrane potential became negative, the $CR_{w\text{-}i}$ values increased significantly and the contribution of cycle *F* and *I* predominated (Fig. 5E, 6B). Near the resting membrane potentials, cycle *A* is no longer the predominant cycle. This behavior in an asymmetric condition has not been attained from experiments since most of the measurements including V_{stream} are basically performed under symmetrical conditions.

The voltage-dependency of the relative contribution of the cycles in the asymmetric ion condition gives an insight how ions and water molecules are queued in physiologically relevant conditions. This prediction is based on the permeation model having a symmetric

potential profile (Materials and Methods), reflected from the nearly symmetrical distributions of K^+ in the four binding sites of the selectivity filter (Zhou and MacKinnon, 2003). Introducing asymmetry (Treptow and Tarek, 2006) in the potential profile is the topics of the future trials.

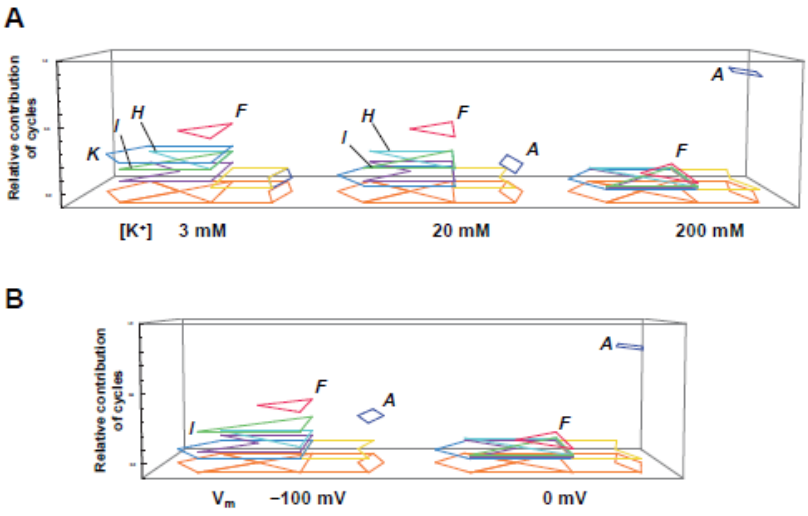

Fig. 6. Visualized permeation processes **A.** The relative contributions of cycles at different K^+ concentrations. The 8-state diagram is shown as the footprint, above which cyclic paths predominantly used in the permeation are demonstrated (The dark blue diamond for cycle *A*, the red triangle for cycle *F*). The relative contributions of cycles are expressed as the level of height raised from the footprint. Cycles contributing to the net flux below 0.01 were not shown. At 200 mM, the relative contribution of cycle *A* was 0.83, and cycle *F* was 0.15; At 20 mM, cycle *A* was 0.29, cycle *F* was 0.42, cycle *G* was 0.03, and cycle *H* and I were 0.11; At 3 mM, cycle *A* was 0.04, cycle *F* was 0.34, cycle *G* was 0.09, cycle *H* and *I* were 0.18, cycle *K* was 0.13, and cycle *L* was 0.03. **B.** Predicted relative contributions of cycles at different membrane potentials in an asymmetric condition of 4 mM K_{out} and 150 mM K_{in}. At 0 mV, the relative contribution of cycle *A* was 0.62, cycle *F* was 0.22, cycle *H* was 0.01, cycle *I* was 0.11, and cycle *L* was 0.02; At -100 mV, cycle *A* was 0.34, cycle *F* was 0.38, cycle *G* was 0.02, cycle *H* was 0.03, cycle *I* was 0.22, and cycle *L* was 0.02.

Discussion

In this study we measured the V_{stream} values as small as 0.5 mV. This value is smaller than those measured ever since the first reports of V_{stream} for the gramicidin channel in 1978 (Levitt et al., 1978; Rosenberg and Finkelstein, 1978). Before discussing the underlying mechanism of permeation refered from our measured results, we start from evaluating the experimental accuracy of the $CR_{w\text{-}i}$ values and the validity of the permeation model.

Detecting such small changes attributes to our method setting appropriate reference points rather than the earlier methods correcting several indipendent factors to reach the results. For example, in our measurements the liquid junction potential arises between different osmolality solutions from the double-burrel tube. By placing the reference electrode close to the patch electrode, this junction potential needs not to be concerned. Also slowly developing concentration polarization, which contributes substantially in the steady-state measurements of V_{stream}, was nulled by measuring the voltage change immediately upon exposure to the osmotic gradient using the rapid osmotic jump method. The overall accuracy of our measurements falls below 0.1 mV in V_{stream}.

The 8-state permeation model is based on the ion distribution on the crystal structure of the KcsA channel (Fig. 1A,B), giving realistic pictures of ion permeation process that has not been attained in the before-crystal age. The 8-state model encompasses the all possible configurations of the ion distribution in the selectivity filter provided that positioning ions in adjacent sites are not allowed. During permeation, a queue of ion and water flow takes one of the occupying states, and transitions among the states generate the cyclic paths on the diagram giving the cycle flux of defined number of ion and water flow (Fig. 1C,D). Thus, this diagram connects the crystal data and dynamic permeation processes. Recently, studies of computer simulation suggested other arrays of ions and water molecules in the selectivity filter (Jensen et al., 2010). Two issues were raised as to whether ions may or may not be located adjacently, and whether or not five sites rather than four sites in the selectivity filter should be considered. There is no experimental evidence for and against the proposal. Measurements of V_{stream} potentially provide clues to such questions. For example, the $CR_{w\text{-}i}$ value at the higher extreme of K^+ concentration gives the maximal number of ions loaded in the single-file region of the selectivity filter. These experiments are, however, more difficult than that of the present study, and we reserve such experiments for future study and use the canonical 8-state model.

To interpret the $CR_{w\text{-}i}$ value, the possible contribution of the intracellular entryway was considered, where water flux carries ions, even in the outside of the single-file region, to generate water-ion

coupling. We estimated the $CR_{w\text{-}i}$ value of the wide pore region for the first time by using the Levitt theory. The relevant L_p value for the empty pore (L_0) was taken from that of the gramicidin channel exhibiting similar geometry of the single-file pore. Using the probability of the empty pore (f_0) at different K^+ concentrations, the estimation revealed that the $CR_{w\text{-}i}$ value for the wide pore is negligible in the KcsA channel.

To attain a realistic picture of the ion permeation through the selectivity filter, we assume a view point of Maxwell's demon again, who sits at the outer pore entrance and watches enter and exit traffics of either ion or water molecules. An example of the observed sequence is shown in Fig. 1D. In a queue of ion and water molecules, the demon partitioned into stretches of arrays and assigned them into series of the cyclic paths. Accordingly, a long queue is transformed into a sequence of cycles. Random transitions among states are integrated into cyclic paths having their own completion rate (cycle flux) and the stoichiometric numbers (n_i and n_w), thus, the permeation process can be regarded as random transition among cycles. Sum of these contributed cycles provides macroscopic observable, such as the current amplitude and the $CR_{w\text{-}i}$ value (Eqs. 5 and 6). Thus, the relative contribution of the cyclic paths in a given ionic condition and membrane potential affords an intuitive picture of permeation (Fig. 6). In this way with the electrophysiological experiments and the theoretical analysis, we obtained a view point of the demon, counting ion and water molecules in a streaming queue through the open-filter structure.

Over several decades experimental and theoretical studies have been performed (Hille and Schwarz, 1978; Lauger, 1980; Berneche and Roux, 2001; Morais-Cabral et al., 2001; Thompson et al., 2009; Jensen et al., 2010). Among them, the “knock-on” mechanism still dominates as an explanation of the permeation processes (Berneche and Roux, 2001; Jensen et al., 2010; Nelson, 2011). One may define the knock-on mechanism as electrostatic repulsion among permeating ions in and out of the pore that drives ion flux efficiently (Hille, 2001). Presence of multiple ions in the pore is prerequisite for the knock-on mechanism. Cycle *A* (Fig. 1B) is the process most suitably explained by the knock-on mechanism. However, our results indicated that cycle *A* appeared in rather limited conditions. As the K^+ concentration was decreased, cycles without passing through the doubly-occupied states increased significantly. Cycle *K*, for example, is a purely one-ion permeation mode, in which there is no way of operating physical knock-on mechanism. Moreover, at an asymmetric concentration similar to physiological conditions, cycle *F* exhibited comparable contributions with cycle *A* for ion flux. In cycle *F*, the transition from state 4 to 3 is not affected by other ions. The knock-on mechanism is physically operated in some of the state transitions on the diagram but not all of them. We conclude that expressing the permeation processes on the diagram using cyclic paths and fluxes is more practical and provide dynamic picture of permeation.

The message of this paper is essentially simple and straightforward. i) Dynamic process such as ion permeation should be examined with dynamic methods. Measuring the currents during the V_{stream} evaluation guarantees that the channel is in the open conformation. Based on the principle of the streaming potential, non-conductive states never contribute to the measured value. ii) Not only ions but also water molecules must be taken into account for elucidating the permeation mechanism. The macroscopic $CR_{w\text{-}i}$ value retains the information how ion and water molecules are queued in the selectivity filter. Thus, measuring the $CR_{w\text{-}i}$ value corresponds to counting the number of individual movements of ion and water molecules through the single-file pore. iii) A mesoscopic view using the cycle flux provides a more intuitive picture of the actual permeation processes (Oiki et al., 2010). Generally, ion permeation through the channel is characterized with various levels of spatial and temporal events in the hierarchy of permeation processes (Dror et al., 2010; Oiki et al., 2010). On one hand, the fine trajectories of ion and water movements in and around the pore have been examined extensively using computational methods (Berneche and Roux, 2001; Jensen et al., 2010). On the other hand, single-channel current data report average number of transferred ions (LeMasurier et al., 2001). Our approach carves out a niche in the study of the permeation mechanism on a scale between the macroscopic current measurements and the elementary steps of ion transfer. Experimental observables were decomposed into linear combinations of cycle fluxes. The permeation is visualized as random transitions among the cycles, each of which exhibits distinct ion and water interplay. We presented here a conceptual framework and the methods for envisioning how the ion and water molecules are queued in single file during permeation.

REFERENCES

Alcayaga C, Cecchi X, Alvarez O, Latorre R (1989) Streaming potential measurements in Ca^{2+}-activated K^+ channels from skeletal and smooth muscle. Coupling of ion and water fluxes. Biophys J 55:367-371.

Ando H, Kuno M, Shimizu H, Muramatsu I, Oiki S (2005) Coupled K^+-water flux through the HERG potassium

channel measured by an osmotic pulse method. J Gen Physiol 126:529-538.
Berneche S, Roux B (2001) Energetics of ion conduction through the K^+ channel. Nature 414:73-77.
Chakrapani S, Cordero-Morales JF, Perozo E (2007) A quantitative description of KcsA gating I: macroscopic currents. J Gen Physiol 130:465-478.
Colquhoun D, Hawkes AG (1995) The principles of the stochastic interpretation of ion-channel mechanisms. In: Single-channel recording, 2nd Edition (Sakmann B, Neher E, eds), pp 397-482. New York: Plenum Press.
Cortes DM, Cuello LG, Perozo E (2001) Molecular architecture of full-length KcsA: role of cytoplasmic domains in ion permeation and activation gating. J Gen Physiol 117:165-180.
Cuello LG, Jogini V, Cortes DM, Perozo E (2010) Structural mechanism of C-type inactivation in K(+) channels. Nature 466:203-208.
Dani JA (1989) Open channel structure and ion binding sites of the nicotinic acetylcholine receptor channel. J Neurosci 9:884-892.
Dani JA, Levitt DG (1981) Water transport and ion-water interaction in the gramicidin channel. Biophys J 35:501-508.
Delcour AH, Martinac B, Adler J, Kung C (1989) Modified reconstitution method used in patch-clamp studies of Escherichia coli ion channels. Biophys J 56:631-636.
Doyle DA, Morais Cabral J, Pfuetzner RA, Kuo A, Gulbis JM, Cohen SL, Chait BT, MacKinnon R (1998) The structure of the potassium channel: molecular basis of K+ conduction and selectivity. Science 280:69-77.
Dror RO, Jensen MO, Borhani DW, Shaw DE (2010) Exploring atomic resolution physiology on a femtosecond to millisecond timescale using molecular dynamics simulations. J Gen Physiol 135:555-562.
Eisenman G, Latorre R, Miller C (1986) Multi-ion conduction and selectivity in the high-conductance Ca^{++}-activated K^+ channel from skeletal muscle. Biophys J 50:1025-1034.
Hill TL (1988) Interrelations between random walks on diagrams (graphs) with and without cycles. Proc Natl Acad Sci U S A 85:2879-2883.
Hill TL (2004) Free Energy Transduction and Biochemical Cycle Kinetics. New York: Dover Publications, Inc.
Hille B (2001) Ion Channels of Excitable Membranes, Third edition Edition. MA: Sinauer Associated, Inc.
Hille B, Schwarz W (1978) Potassium channels as multi-ion single-file pores. J Gen Physiol 72:409-442.
Hodgkin AL, Keynes RD (1955) The potassium permeability of a giant nerve fibre. J Physiol 128:61-88.
Ismailov, II, Shlyonsky VG, Benos DJ (1997) Streaming potential measurements in alphabetagamma-rat epithelial Na+ channel in planar lipid bilayers. Proc Natl Acad Sci U S A 94:7651-7654.
Iwamoto M, Shimizu H, Inoue F, Konno T, Sasaki YC, Oiki S (2006) Surface structure and its dynamic rearrangements of the KcsA potassium channel upon gating and tetrabutylammonium blocking. J Biol Chem 281:28379-28386.
Jensen MO, Borhani DW, Lindorff-Larsen K, Maragakis P, Jogini V, Eastwood MP, Dror RO, Shaw DE (2010) Principles of conduction and hydrophobic gating in K+ channels. Proc Natl Acad Sci U S A 107:5833-5838.
Katchalsky A, Curran PF (1965) Nonequilibrium Thermodynamics in biophysics. Cambridge: Harvard University Press.
Kuno M, Ando H, Morihata H, Sakai H, Mori H, Sawada M, Oiki S (2009) Temperature dependence of proton permeation through a voltage-gated proton channel. J Gen Physiol 134:191-205.
Lauger P (1980) Kinetic properties of ion carriers and channels. J Membr Biol 57:163-178.
LeMasurier M, Heginbotham L, Miller C (2001) KcsA: it's a potassium channel. J Gen Physiol 118:303-314.
Levitt DG (1984) Kinetics of Movement in Narro Channels. Current Topics in Membranes and Transport 21:181-197.
Levitt DG (1990) Streaming potential: Continuum expression applicable to very small nonuniform ion channels. J Chem Phys 92:6953-6957.
Levitt DG, Elias SR, Hautman JM (1978) Number of water molecules coupled to the transport of sodium, potassium and hydrogen ions via gramicidin, nonactin or valinomycin. Biochim Biophys Acta 512:436-451.
Lockless SW, Zhou M, MacKinnon R (2007) Structural and thermodynamic properties of selective ion binding in a K+ channel. PLoS Biol 5:e121.
Miller C (1982) Coupling of water and ion fluxes in a K+-selective channel of sarcoplasmic reticulum. Biophys J 38:227-230.
Miller C (1999) Ionic hopping defended. J Gen Physiol 113:783-787.
Morais-Cabral JH, Zhou Y, MacKinnon R (2001) Energetic optimization of ion conduction rate by the K+ selectivity filter. Nature 414:37-42.
Nelson PH (2011) A permeation theory for single-file ion channels: One- and two-step models. J Chem Phys 134:165102.
Oiki S, Iwamoto M, Sumikama T (2010) A mesoscopic approach to understanding the mechanisms underlying the ion permeation on the discrete-state diagram. J Gen Physiol 136:363-365.
Oiki S, Iwamoto M, Sumikama T (2011) Cycle Flux Algebra for Ion and Water Flux through the KcsA Channel Single-file Pore Links Microscopic Trajectories and Macroscopic Observables. PLoS ONE 6:e16578.
Rosenberg PA, Finkelstein A (1978) Interaction of ions and water in gramicidin A channels: streaming potentials across lipid bilayer membranes. J Gen Physiol 72:327-340.

Saparov SM, Pohl P (2004) Beyond the diffusion limit: Water flow through the empty bacterial potassium channel. Proc Natl Acad Sci U S A 101:4805-4809.

Schulz SG (1980) Basic Principles of Membrane Transport. Cambridge: Cambridge University Press.

Thompson AN, Kim I, Panosian TD, Iverson TM, Allen TW, Nimigean CM (2009) Mechanism of potassium-channel selectivity revealed by Na(+) and Li(+) binding sites within the KcsA pore. Nat Struct Mol Biol 16:1317-1324.

Treptow W, Tarek M (2006) K+ conduction in the selectivity filter of potassium channels is monitored by the charge distribution along their sequence. Biophys J 91:L81-83.

Zhou M, MacKinnon R (2004) A mutant KcsA K(+) channel with altered conduction properties and selectivity filter ion distribution. J Mol Biol 338:839-846.

Zhou Y, MacKinnon R (2003) The occupancy of ions in the K+ selectivity filter: charge balance and coupling of ion binding to a protein conformational change underlie high conduction rates. J Mol Biol 333:965-975.

Zhou Y, Morais-Cabral JH, Kaufman A, MacKinnon R (2001) Chemistry of ion coordination and hydration revealed by a K+ channel-Fab complex at 2.0 A resolution. Nature 414:43-48.

In parallel, we must consider possible contribution of the pore region outside the selectivity filter. In the intracellular entryway towards the central cavity for the open structure with the geometry of about 5-6 A in the radius, osmotically driven water flux carries ions and this contributes to the measured $CR_{w\text{-}i}$. Levitt proposed a theoretical method to estimate the coupling outside the single-file region of the pore. The water flux is rate-limited at the selectivity filter and this flow determines the degree of coupling given the geometry of the entryway. In addition, the flux rate of water (or rather expressed as the hydraulic conductivity coefficient, L_p) depends on the occupancy of the ion in the selectivity filter, and the overall L_p value is determined as,

$$L_p = f_0 L_0 + f_1 L_1 + f_2 L_2 + \ldots$$

where f_0, f_1, f_2 etc. are the fraction of channels that contain zero, one, two, etc. ions and L_0, L_1, L_2 etc. are the hydraulic water conductivity for channels containing zero, one, two, etc. ions. Unfortunately, these data are ing into account the Lp value for the empty pore .

Validating this model is an important issue. In this model, we first assumed that water-ion coupling occurs exclusively in the narrow selectivity filter. The estimated contribution of the intracellular entryway to the measured $CR_{w\text{-}i}$ based on the Levitt theory and the relevant L_p value, demonstrated that the above assumption is acceptable. At low K, if the L_o value of the KcsA channel is ten times higher than expected, then, the contribution of the wide pore becomes 0.1 out of the measured $CR_{w\text{-}i}$ value of 2.2.

Next, a question of the validity for the 8-state diagram includes a possibility that ions in the selectivity filter may occupancy adjacently. If it is the case, up to four ions may occupy the selectivity filter simultaneously. Experimental verification of the 8-state model is not easy. However, studies of computer simulation have provided some clues. For example, Jensen et al. exhibited that the $CR_{w\text{-}i}$ was close to one at 600 mM K solution for the Kv channel, supporting only two ions occupy the filter as proposed by the 8-state model. not available for the KcsA channel. To estimate a realistic value of the contribution of the entryway, we adopted the L_p values for gramicidin channels exhibiting single-file permeation, in which not only the L_0 but L_1 and L_2 are available (Ref.). Also, from our model, f0, f1 and f2 are calculated. Given the Pf value of 6.0×10^{-14} cm^3/s for L_0, 1.3×10^{-14} cm^3/s for L_1 and 1.0×10^{-15} cm^3/s for L_2 (ref. Dani & Levitt) and the probability of channels containing defined number of ions at different ion concentrations, the coupling ratio was estimated to be 0.02 at 200 mM K+ and 0.05 at 3 mM K+. If the Lp value for the KcsA channel is five times higher than that of the gramicidin channel, the $CR_{w\text{-}i}$ value for the selectivity filter becomes 0.9 at 200 mM K.

The validity of the assumption is in principle proven using the streaming potential. One may have a clue that the preposition of the electrically unfavored close apposition may be true or not, if $CR_{w\text{-}i}$ becomes less than 1/3. Alternatively, three ions separated by water molecules can fit in the selectivity filter, if $CR_{w\text{-}i}$ is 2/3. However, practically these measurements are difficult and need to wait for the future trials. On the other hand, recent computer simulation runs permeation processes and revealed the $CR_{w\text{-}i}$ value close to 1.0 at 600 mM K.

We need to wait future trials.

than expressing the mode of permeation with the simple key word of “knock-on”.

Validating this model is an important issue. In this model, we first assumed that water-ion coupling occurs exclusively in the narrow selectivity filter. Then, we examined the possible contribution of the wide channel region for the measured $CR_{w\text{-}i}$ value. We applied Levitt’s theory to estimate the contribution of the intracellular entryway. In the application of the theory, it should be taken into account that osmotically driven water flow is stopped for the ion occupied pores in the experimental condition for the V_{stream} measurements (D&L). Thus, the L_0 value in Eq. 3 is necessary for estimating the contribution of the wide pore. We applied the L_o value of the gramicidin channel. Although this L_p value may not reflect that of KcsA channel, the low probability of the empty channel in high K concentration nulled the effect of the wide pore at least at high K concentrations. At low K, if the L_o value of the KcsA channel is ten times higher than expected, then, the contribution of the wide pore becomes 0.1 and the $CR_{w\text{-}i}$ value of the selectivity filter should be 2.1.

In parallel to this realistic view, we are presenting a novel view point of the permeation on the permeation diagram (Fig. 6). Experimentally observed current amplitudes and $CR_{w\text{-}i}$ are results of random transitions on the premeation diagram. Random transitions among states are integrated into cyclic paths having their own completion rate (cycle flux) and the stoichiometric numbers (n_i and n_w). The current amplitudes and $CR_{w\text{-}i}$

are expressed as the weighted sum of each cycle flux. Thus, the permeation is regarded as transitions among the cyclic paths, and the relative contribution of the cyclic paths in a given ionic condition and membrane potential affords an intuitive picture of permeation (Fig. 6). In this way with the electrophysiological experiments and the theoretical analysis, we obtained a view point of the demon, counting ion and water molecules in a streaming queue through the open-filter structure.

Detecting such small changes owe to our method relying on the appropriate setting of the reference point rather than the earlier methods correcting several indipendent factors to reach the results.